

ATR-Mapping: Asymmetric Topological Representation based Mapping Framework for Multi-Robot Environment Exploration

Hao Zhang, Jiyu Cheng, and Wei Zhang, *Senior Member, IEEE*

Abstract—In recent years, the widespread application of multi-robot systems in areas such as power inspection, autonomous vehicle fleets has made multi-robot technology a research hotspot in the field of robotics. This paper investigates multi-robot cooperative exploration in unknown environments, proposing a training framework and decision strategy based on multi-agent reinforcement learning. Specifically we propose a Asymmetric Topological Representation based mapping framework (ATR-Mapping), combining the advantages of methods based on raw grid maps and methods based on topology, the structural information from the raw grid maps is extracted and combined with a topological graph constructed based on geometric distance information for decision-making. Leveraging this topological graph representation, we employs a decision network based on topological graph matching to assign corresponding boundary points to each robot as long-term target points for decision-making. We conducts testing and application of the proposed algorithms in real world scenarios using the Gazebo and Gibson simulation environments. It validates that the proposed method, when compared to existing methods, achieves a certain degree of performance improvement.

Index Terms—Multi-robot system; multi-robot exploration; multi-agent reinforcement learning; graph neural network

I. INTRODUCTION

WITH the advancement of artificial intelligence technology, the global manufacturing industry has entered a new stage characterized by intelligence and informatization. Multi-robot technology no longer confines itself to the independent operation of a single robot but instead involves multiple robots working together to achieve more efficient task execution. For instance, in the industrial sector, multi-robot collaborative systems can adapt to dynamically changing production demands, enhancing the productivity and flexibility of production lines [17]. In the service sector, multi-robot systems can also collaborate to accomplish various complex tasks such as unmanned logistics [6], smart transportation [21], and so on. Moreover, in emergency situations like disaster relief efforts, multi-robot systems can rapidly respond and collaborate to perform tasks such as search and rescue [9], thereby improving the efficiency and safety of emergency response.

However, in applications such as search and rescue, as well as inspection [13], multiple robots cannot obtain environment map information in advance and need to operate in unknown environments. Therefore, multi-robot exploration of unknown environments, as one of the basic tasks of mobile multi-robot systems, is also a research hotspot in the field of multi-robotics. In the task of multi-robot exploration of unknown environments, multiple robots need to locally perceive structural information of the workspace through sensors they carry, communicate with fellow robots under certain conditions, make collaborative decisions, and then reconstruct the environment model accurately and quickly during the movement process.

This paper proposes a multi-robot active mapping method called ATR-Mapping, including an asymmetric structured feature extraction module and a decision module based on topological map matching. The module encodes observation features using a differential structured feature extraction network and generates state values by capturing the difference between privileged observation information and observation information. The main contributions are summarized as follows:

- We proposes an asymmetric feature representation framework. The differential structured feature extraction network obtains feature mappings from observed and privileged observed information. The asymmetric actor-critic training framework uses the exploration rate error as additional supervision to train the value loss function in reinforcement learning.
- The multi-agent decision-making method using topological graph matching based on the asymmetric feature representation framework. It includes a feature extraction method using bilinear interpolation and boundary point clustering. The decision network framework uses topological graph matching to match the robot's representation with the boundary point's representation.
- A training environment using OpenAI Gym for deep reinforcement learning. The algorithm is trained, deployed, and tested in a simulated environment. Additionally, the algorithm is deployed and tested in the Gazebo and iGibson simulation environments to showcase its practicality and potential application in real-world scenarios.

The rest of this article is organized as follows. Section II introduces some related works as well as their advantages and disadvantages. Section III gives the problem formulation of

Hao Zhang, Jiyu Cheng, and Wei Zhang are with the School of Control Science and Engineering, Shandong University, Jinan 250061, China (e-mail: hao.zhang@mail.sdu.edu.cn; {jycheng, davidzhang}@sdu.edu.cn).
(Corresponding author: Jiyu Cheng.)

the task. Section IV describes the details of our framework. The experiment implementation and the analysis of the results are presented in Section V. Finally, Section VI draws the conclusions and gives our future work.

II. RELATED WORK

In the task of multi-robot exploration of unknown environments, the boundary points of known and unknown maps play a crucial role in robot decision-making. In cooperative decision-making algorithms for multi-robot exploration of unknown environments, the core task is to allocate target points for robots and determine their direction of movement based on boundary point information to complete the exploration of enclosed spaces as quickly as possible. Below, we will provide a detailed analysis and introduction of existing methods for these categories.

A. Methods Based on Classical Optimization Algorithms

Heuristic methods are strategies based on human experience and intuition, aiming to quickly generate approximate optimal target point allocation methods. In multi-robot exploration of unknown environments, the most intuitive decision-making strategy is for each robot to move towards the nearest boundary point. In the early research on multi-robot cooperative exploration tasks, Yamauchi et al. [18] proposed a distance greedy algorithm based on this idea, which allocates boundary points to each robot as movement target points based on the nearest distance heuristic principle. Meanwhile, Juliá et al. [10] introduced the concept of information gain associated with boundary points—i.e., the area of unexplored regions within a certain range near the boundary points—and proposed a greedy algorithm based on information gain, where each robot moves towards several boundary points with the maximum information gain. However, although the above two types of greedy algorithms can ensure the complete exploration of the map, they often lead to redundant exploration among multiple robots in practice due to the lack of high-level coordination consideration. To address this, Colares et al. [3] designed a utility function that simultaneously considers information gain and distance from boundary points to describe the exploration value of boundary points, and introduced collaborative factors among multiple robots to achieve more efficient target point allocation. Bourgault et al. [3], on the other hand, considered scene segmentation and introduced Voronoi segmentation to divide the entire map with robots as seed points. After segmentation, each robot selects the nearest boundary point in its respective subspace as a movement target point, thereby avoiding redundant exploration of the environment among multiple robots.

Another commonly used heuristic method in the field of multi-robot exploration of unknown environments is based on the artificial potential field (APF) method, which is a heuristic approach based on manually designed rules that set up virtual force fields to attract or repel robot movement in the scene. Robots are attracted to targets while being repelled by obstacles, allowing them to quickly reach the goal while avoiding obstacles. The artificial potential field method was

initially used in global path planning for target navigation tasks in mobile robotics [3]. In this potential field, obstacles are set with high potential energy, while target points have low potential energy. Therefore, robots move towards the target points along the direction of maximum potential energy descent in the field. Obviously, if the potential field is properly established, this method can also be used for multi-robot exploration tasks of unknown environments. In early research, Lau et al. [11] constructed a potential energy function based on distance values, setting robots and obstacles as high potential points and boundary points as low potential points, and assigned different proportion coefficients to different entities to guide robots in the correct direction. However, simply using a potential energy function based on Euclidean distance can lead to the problem of local minima, where robots may get trapped in certain unexpected local minima points. To address this, Renzaglia et al. [14] applied artificial potential fields to local navigation in multi-robot exploration of unknown environments and introduced a greedy algorithm for boundary points to overcome the local minima problem. Meanwhile, Liu et al. [12] discretized the environment into a grid, designed a nonlinear potential energy function, and introduced the concept of coverage factor to promote cooperative exploration among robots while solving the local minima problem. In recent years, Yu et al. [20] introduced a new wavefront distance based on the length of the robot-to-boundary point path to construct a potential field function to address the local minima problem, and used the overlapping coverage area of sensors of multiple robots as a penalty function to reduce redundant exploration and improve decision-making efficiency.

B. Learning-Based Methods

In recent years, with the development of deep reinforcement learning and multi-agent reinforcement learning theories, learning-based methods for multi-robot exploration of unknown environments have gradually become a hot research topic in academia. Learning-based methods in multi-robot exploration of unknown environments are mainly based on deep reinforcement learning and its extension forms. Methods based on deep reinforcement learning iteratively interact with the environment to obtain reward values as supervised signals to train value networks and policy networks, making them approximate optimal decisions. In the early methods based on reinforcement learning, researchers mainly considered discretized grid map scenarios. In these scenarios, the robot's observation is represented as a grid map, and the robot's actions are movements at the grid level. Geng et al. [7] proposed a decentralized decision-making method based on multi-agent reinforcement learning in grid map environments, where multiple robots exchange observation information encoded by convolutional neural networks through learnable network structures to achieve collaborative decision-making. Subsequently, Geng et al. [8] further improved the multi-robot communication module and introduced attention mechanisms to achieve more purposeful information exchange. However, the short-sighted action space of robots in grid maps can lead to poor performance of trained models in long-term decision-making. Therefore, Tan et al. [16] introduced hierarchical

reinforcement learning, extending the decision model into a hierarchical decision-making form. In this form, the upper-level policy is responsible for allocating long-term forward target positions for the robots, while the lower-level policy is responsible for generating low-level actions at the grid level. By introducing hierarchical decision-making, the collaboration among multiple robots and the ability for long-term decision-making are enhanced to a certain extent.

III. PROBLEM FORMULATION

During the exploration process, this paper adopts a discrete time step and discrete action setting, where each robot can only move to adjacent grid cells at each time step. Once a key cell in the environment is visited by any robot, it becomes a regular free cell. Therefore, for the progressively detailed multi-robot exploration task, the objective is to visit as many key cells as possible within a limited time constraint. Specifically, the task can be formulated as finding an optimal policy π^* that maximizes the objective function.

$$\pi^* = \arg \max_{\pi} \sum_{t=0}^T \sum_{i \in R, j \in C_t} c_t^j \Pi_{q_t^i = p^j} \quad (1)$$

$$s.t. c_t^j = \begin{cases} 0 & \text{if } q_t^i = p^j \forall \tau < t, j \in C_t, i \in R \\ 1 & \end{cases} \quad (2)$$

$$\{q_t^i\}_{i \in R} = \pi(W_{t-1}, C_{t-1}, F_{t-1}, R) \quad (3)$$

where R , W_t and C_t representing the robots, free cells, and key cells, respectively. F_t representing the boundary cells at time t . T representing Time budget for the task. q_t^i and p^j representing the positions of robot i and accessible cell j (accessible cells include free cells, boundary cells, and key cells) at time t . c_t^j representing variable indicating whether accessible cell j is a key cell. $\Pi_{q_t^i = p^j}$ representing indicator function representing whether robot i has reached accessible cell j at time t .

A. Modeling of Markov Decision Process

The main task addressed in this chapter is the long-term goal selection task in the multi-robot active mapping mission. Considering an indoor scenario with convenient communication, a centralized decision-making approach is adopted. In this scenario, the multi-robot active mapping task can be modeled as a centralized Partially Observable Markov Decision Process (POMDP). This process can be represented by a tuple $\langle \mathcal{N}, \mathcal{S}, \mathcal{O}, \mathcal{A}, \mathcal{P}, \mathcal{R}, \gamma \rangle$. where \mathcal{N} is the set of N agents (robots). \mathcal{S} represents the global state space. $\mathcal{O} = \times_{i \in \mathcal{N}} \mathcal{O}_i$ is the joint observation space for multiple robots, where \mathcal{O}_i is the observation function. $\mathcal{A} = \times_{i \in \mathcal{N}} \mathcal{A}_i$ represents the joint action space for multiple robots. $\mathcal{P} : \mathcal{S} \times \mathcal{A} \rightarrow \Delta(\mathcal{S})$ denotes the state transition probabilities. $\mathcal{R} : \mathcal{S} \times \mathcal{A} \rightarrow \mathbb{R}$, is the reward function for all agents. $\gamma \in [0, 1)$ is the reward discount factor. At each time step, agents receive local observations $o_i^{(t)} = O(S^{(t)}, i)$ from the global state $s^{(t)} \in \mathcal{S}$ then a controller collects observations from all agents and generates a joint action $a^{(t)} = \pi(\cdot | o_1^{(t)}, \dots, o_N^{(t)})$ through a centralized policy. Each agent

receives and executes the corresponding action $a_i^{(t)} \in a^{(t)}$ from the central controller. Finally, the joint actions $a^{(t)} \in \mathcal{A}$ of multiple agents lead the system from state $s^{(t)}$ to state $s^{(t+1)}$ based on the state transition probabilities $P(s^{(t+1)} | a^{(t)})$ and receive reward $r^{(t)} = R(s^{(t)}, a^{(t)})$. To address this problem, value networks and policy networks are designed, employing an end-to-end multi-agent deep reinforcement learning framework. This framework aims to maximize the value function $V_{\pi}(s) = \mathbb{E}_{s,a} [\sum_{t=0}^T \gamma^t r^{(t)} | s_0 = s, a, \pi(\cdot | o_1^{(t)}, \dots, o_N^{(t)})]$ to learn an optimal centralized policy $\pi^*(\cdot | o_1^{(t)}, \dots, o_N^{(t)})$. In the task considered in this chapter, the action space of agents consists of a set of candidate points for long-term goals, where the action of an agent is "selecting a candidate point as a long-term goal and moving towards that target point".

B. Multi-Robot Active Mapping

For a multi-robot collaborative active mapping task, it can be divided into three sub-task modules: perception and map creation, long-term goal selection, and short-term path planning. In the perception and map creation module, robots transform sensor information into 2D grid maps. In the long-term goal selection module, robots allocate and select long-term goal points on the grid maps. In the short-term path planning module, robots plan paths to the selected long-term goal points. The overall task framework is shown in Fig. 1. The policy network and training algorithm focus on long-term goal selection, while existing methods are used for perception, map creation, and short-term path planning. Detailed descriptions and settings for the three sub-tasks will be provided in the paper.

1) *Perception and Map Creation*: The objective of the perception and map creation module is to construct a global map based on sensor information from multiple robots. Robots use depth cameras as distance sensors, and it is assumed that there is no positioning error. At each time step, the robot converts depth image data into point cloud data in the world coordinate system. Points within the robot's height range are remapped to the top-down 2D map coordinate system, forming an occupancy map centered on the robot. Multiple robots transform their occupancy maps into a common world coordinate system based on their positions and orientation differences, creating a global occupancy map.

In the process of converting depth images to point clouds, this paper adopts homography transformation to perform coordinate transformation between different coordinate systems. Specifically, at each time step, the robot obtains a depth image $I_i^{(t)} \in \mathbb{R}^{h \times w}$ and the global pose $L_i^{(t)} \in \mathbb{R}^3$ from the environment. For any point (u, v) in the depth image, assuming its corresponding point cloud coordinates in the world coordinate system are represented as (x, y, z) , the relationship between them can be described as follows:

$$\begin{bmatrix} u \\ v \\ 1 \end{bmatrix} = \frac{1}{z_c} K \cdot \begin{bmatrix} R & t \end{bmatrix} \begin{bmatrix} x \\ y \\ z \\ 1 \end{bmatrix} \quad (4)$$

Where $R \in \mathbb{R}^{3 \times 3}$ and $t \in \mathbb{R}^{3 \times 1}$ are respectively the rotation matrix and translation matrix in the extrinsic parameter

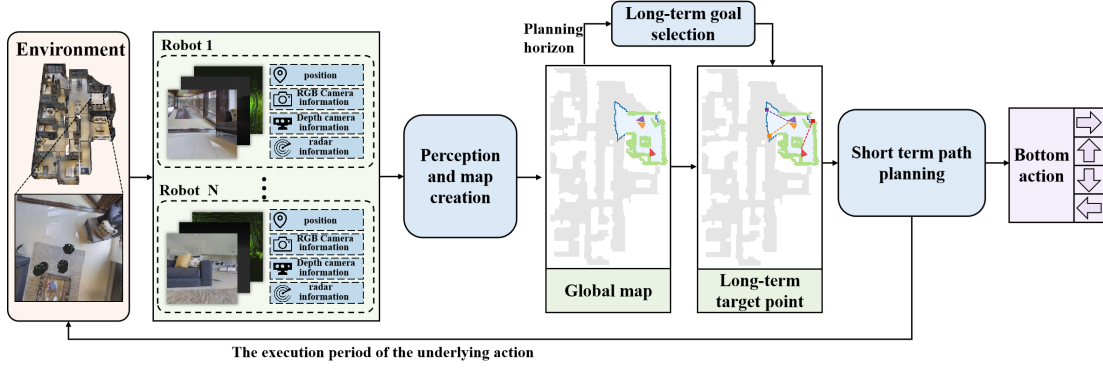


Fig. 1. Multi-robot collaborative active mapping task framework, three main sub-modules: perception and map creation, long-term goal selection, and short-term path planning.

matrix, z_c is the value of the z-axis in camera coordinates, i.e., the depth value of point (u, v) , and K is the camera's intrinsic matrix, which can be represented as:

$$K = \begin{bmatrix} f_x & S & C_x \\ 0 & f_y & c_y \\ 0 & 0 & 1 \end{bmatrix} \quad (5)$$

Where f_x and f_y refer to the focal lengths in the horizontal and vertical directions of the camera, respectively, c_x and c_y denote the pixel differences between the image origin and the image center along the horizontal and vertical axes, respectively. S represents skewness errors caused by manufacturing processes of the camera, typically set to 0 in most cases.

In the setup of this paper, each robot first establishes a 3D point cloud centered around itself based on the depth image. Therefore, the world coordinate origin and the camera origin coincide. The rotation matrix R and the translation matrix t can be represented as:

$$R = \begin{bmatrix} 0 & 0 & 0 \\ 0 & 1 & 0 \\ 0 & 0 & 1 \end{bmatrix}, t = \begin{bmatrix} 0 \\ 0 \\ 0 \end{bmatrix} \quad (6)$$

Furthermore, in this paper, the image origin coincides with the image center, so $c_x = c_y = 0$. Therefore, substituting the corresponding values and transforming Equation (4), we obtain:

$$\begin{bmatrix} x \\ y \\ z \end{bmatrix} = z_t \begin{bmatrix} \frac{1}{f_x} & 0 & 0 \\ 0 & \frac{1}{f_y} & 0 \\ 0 & 0 & 1 \end{bmatrix} \begin{bmatrix} u \\ v \\ 1 \end{bmatrix} \quad (7)$$

After the transformation described above, each pixel in the depth image $I_i^{(t)}$ is converted into a point in the 3D point cloud. The resulting point cloud can be represented as $P_t^{(t)} = \{P_k | k = 1, 2, 3, \dots, h \cdot w\}$, where $P_k = (x, y, z)$ denotes the position of the corresponding point in the world coordinate system with the robot as the origin (for ease of subsequent representation, this paper swaps the y-axis and z-axis obtained from the coordinate transformation, making the x-y plane correspond to the parallel horizontal plane of robot movement). The perception and mapping module aims

to construct a top-down 2D map to describe environmental features. Therefore, this paper utilizes an occupancy grid map to represent the 2D map. The occupied grid map of robot i at time t can be denoted as $M_t^{(t)} \in \{0, 1\}^{X_l \times Y_l \times 2}$. Here, X_l and Y_l represent the predetermined map dimensions, and the two map channels respectively indicate the explored and occupied areas. Thus, each grid point in the grid map can be classified into one of three categories: open (explored but unoccupied), occupied, and unknown (unexplored). The mapping task in this paper only considers obstacles that obstruct robot movement, specifically obstacles within the height range of the robot itself. Specifically, if the grid map resolution is r_s and the robot height is h_r , then for any point k in the point cloud, its corresponding coordinates in the grid map are (m, n) , where $m = \lfloor P_k(1)/r_s \rfloor$ and $n = \lfloor P_k(2)/r_s \rfloor$. Therefore, $M_i^{(t)}(m, n)$ can be expressed as:

$$M_i^t(m, n) = \begin{cases} [1, 1] & \text{if } 0 < P_k(3) < h_r \\ [1, 0] & \text{if } P_k(3) \leq 0 \text{ or } P_k(3) > h_r \end{cases} \quad (8)$$

In this way, each of the N robots in the scene obtains an occupancy grid map centered around itself. Multiple robots exchange information to output their own poses $L_i^t = (x, y, \theta)$ and occupancy grid maps M_i^t . Each robot transforms its respective grid map to the common world coordinate system based on its pose and merges it with the previous global grid map $M^{(t-1)}$ to obtain the global grid map $M^{(t)}$ at time t .

2) *Long-term Goal Selection*: In long-term goal selection, one straightforward choice is for each robot to move toward the boundaries of the known and unknown map areas at each time step. As long as robots continuously move toward boundary points, and assuming the map is closed and bounded, robots will eventually complete exploration of the environment. This method based on boundary points is also adopted in this paper. Therefore, the goal of the long-term goal selection module is to assign a boundary point as a long-term target point for each robot when each planning cycle arrives, allowing multiple robots to explore as much of the unknown environment as possible in the shortest possible time and ultimately establish a global grid map containing

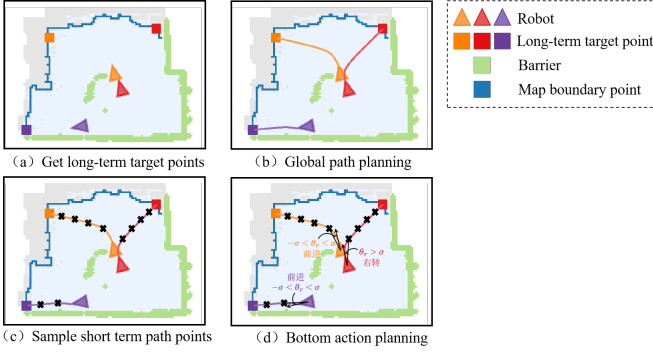


Fig. 2. Short-term path planning schematic.

all environmental information. Finally, when there are no reachable boundary points in the scene, it is considered that the robots have completed full exploration of the environment, and the task ends.

3) *Short-term Path Planning*: Short-term path planning is a discretized subtask in which robots, after receiving long-term goals, individually plan the shortest paths to reach their respective targets based on the global grid map $M^{(t)}$. The entire short-term path planning process is illustrated in Fig. 2. In this paper, the Fast Marching Algorithm [15] is adopted to compute the shortest path from the robot's position to the target position. After obtaining the shortest path in the grid map, it needs to be translated into low-level actions for execution by the lower-level actuators. The shortest path points obtained based on the grid map are downsampled at a certain density, and the closest point to the robot after downsampling is selected as the short-term path point. Upon obtaining the short-term path points, robots generate low-level actions through a simple heuristic method [2]: if a robot is facing the path point, it executes a forward action; otherwise, it performs rotation actions until it faces the path point and then moves forward.

Specifically, the relative angle θ_r is calculated by subtracting the direction of the edge pointing to the path point from the robot's orientation to determine whether the robot needs to turn. Therefore, the low-level action $a_i^{(t)}$ for robot i at time t can be obtained as follows:

$$a_i^{(t)} = \begin{cases} \text{turnleft} & \text{if } \theta_r < -\sigma \\ \text{goahead} & \text{if } -\sigma \leq \theta_r \leq \sigma \\ \text{turnright} & \text{if } \theta_r > \sigma \end{cases} \quad (9)$$

Where σ is the angle threshold parameter controlling the robot's turning or straight movement, which is set to $\pi/12$ in this paper.

IV. METHODOLOGY

This paper proposes a multi-robot active mapping method called ATR-Mapping. It integrates grid-based and topological-based approaches, extracting structural information from original grid maps during reinforcement learning training and combining it with topological maps based on geometric distance for decision-making. ATR-Mapping encodes observation

features using a differential structured feature extraction network and generates state values by capturing the difference between privileged observation information and observation information. A loss function predicts unexplored areas to enhance the encoding of structural information. The decision network is improved based on graph matching, and structured features relevant to robots and boundary points are extracted. These features are combined with distance-based geometric topological maps to construct the representation of the topological map. Finally, topological map matching is performed using graph neural networks to allocate boundary points to guide robot movement. The overall framework of the ATR-Mapping method is illustrated in Fig. 3.

A. Asymmetric Feature Representation Framework Design

This section provides an overview of the asymmetric feature representation framework. It consists of two components: a structured feature extraction network and an asymmetric actor-critic training framework. The feature extraction network uses a convolutional neural network to encode robot observation and privileged observation separately. The feature utilization network module generates state values and exploration rate predictions based on the differences between the encoded features. The training framework combines exploration rate prediction error with value loss for training. This allows the network to learn structural information from the differences between observations and privileged information.

1) *Structured Feature Extraction Network Based on Differential Form*: The structured feature extraction network as shown in Fig. 4. The feature encoding network is responsible for encoding and processing observation information and privileged observation information to extract feature mappings. Meanwhile, the feature utilization network needs to utilize the information difference between the feature mappings of observation information and privileged observation information to output state values and exploration rate predictions. To enhance observations by fully utilizing map information and historical data, the global grid map is expanded to a 5-channel map as observation information. The information in the five channels includes obstacle information in explored areas, information on passable areas, positions of all robots, boundary point information, and trajectory information of all robots. Each channel is encoded with 0-1 values, where a grid point value is 1 if there is corresponding entity information, otherwise 0. Specifically, the observation information fed into the structured feature extraction network at each time step is represented as $O_c^{(t)} \in \{0,1\}^{X \times Y \times 5}$, Where X and Y are the dimensions of the global grid map. In addition to observation information, the feature encoding network also needs to encode privileged observation information to obtain feature mappings. Here, privileged information refers to the contour information of all explorable areas obtained directly from the simulator, which includes the passable areas, including unexplored areas, as well as the contour information of obstacles in the entire environment. Therefore, all explorable area information is used to replace the explored area information channel in the observation information, forming privileged

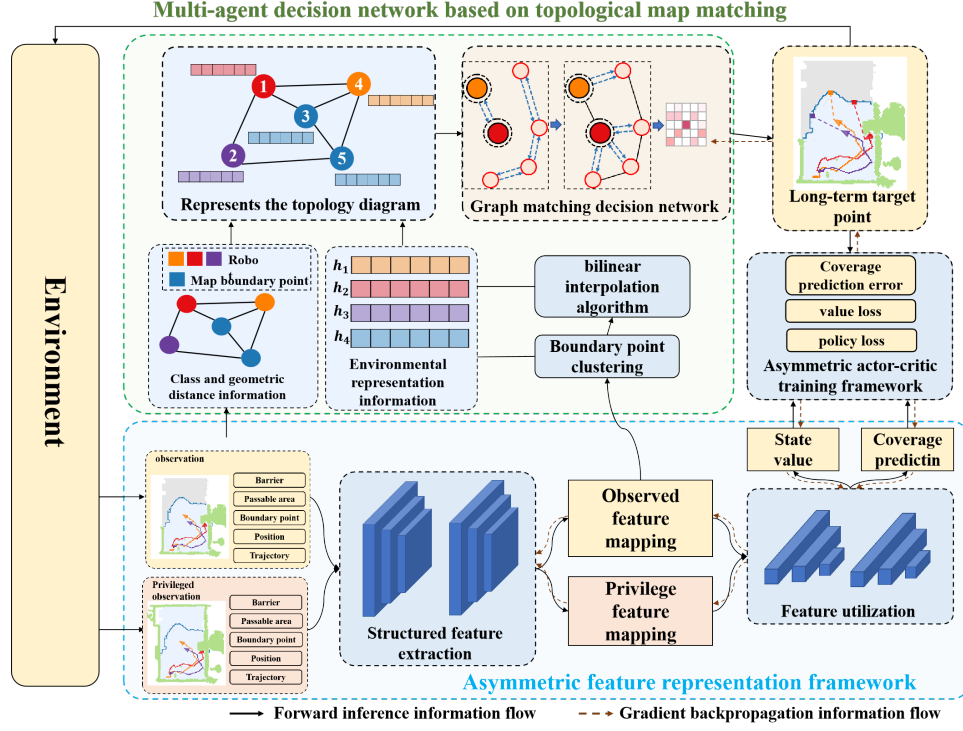


Fig. 3. ATR-Mapping overall frame diagram. ATR-Mapping includes an asymmetric structured feature extraction module and a decision module based on topological map matching. Asymmetric feature representation is used to extract key features from the environment. The multi-agent decision network based on topological map matching includes a representation of the topological map and a graph matching decision network, which is used to generate long-term goal points based on topological map matching.

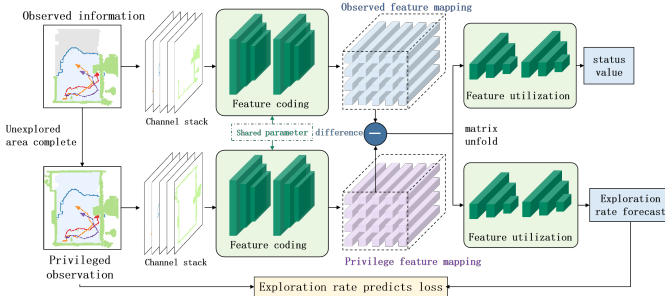


Fig. 4. Structured feature extraction networks based on differential form. The structured feature extraction network based on the differential form consists of two parts: the feature encoding network and the feature utilization network.

observation information. For privileged observation information, its five channels are global obstacle information, global passable area information, positions of all robots, boundary point information, and trajectory information of all robots, represented as $\hat{O}_c^{(t)} \in \{0, 1\}^{X \times Y \times 5}$. The visualization of each channel in privileged observation information and observation information is shown in Fig. 5.

After obtaining observation information and privileged observation information, this paper designs an encoder with a convolutional neural network (CNN) as the backbone, serving as the feature encoding network. The network consists of several layers of convolutional neural networks and activation functions concatenated together. The feature encoding network performs dimensionality reduction on the input observation in-

formation while increasing the number of channels, extracting structured features from the spatial domain into corresponding channel vectors. If the input size is $X \times Y \times 5$, the output feature mapping size is $X_h \times Y_h \times C_h$, where $X_h = X/8$, $Y_h = Y/8$, and $C_h = 32$ are selected in this paper. At time t , the privileged observation information and observation information, after feature extraction by the aforementioned feature encoding network, yield privileged feature mappings $\hat{F}_c^{(t)} \in \mathbb{R}^{X_h \times Y_h \times C_h}$ and observation feature mappings $F_c^{(t)} \in \mathbb{R}^{X_h \times Y_h \times C_h}$ respectively. The size of privileged feature mappings and observation feature mappings are the same, differing only in whether the channel information representing explored areas includes privileged information. Therefore, the difference between privileged feature mappings and observation feature mappings contains not only the overall area difference between explored and unexplored areas but also the structured feature information of obstacle distribution in the environment. Consequently, this paper utilizes the difference between privileged feature mappings and observation feature mappings as input to the feature utilization network to predict the state value of the current state. Additionally, to ensure that the feature encoding network correctly captures the structured feature information reflected in the difference between privileged feature mappings and observation feature mappings, this paper introduces the prediction of the current exploration rate as one of the network's outputs. Finally, the gradient is backpropagated to the feature encoding network for training through the corresponding loss function. Therefore, the input to the feature utilization network is the difference between privileged feature

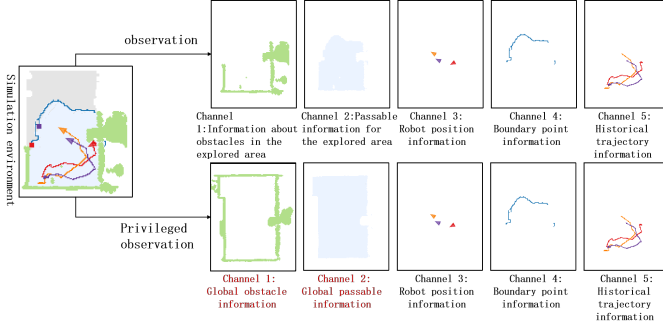


Fig. 5. Channels of observational information and privileged observational information.

mappings and observation feature mappings, and the difference feature mappings are flattened into one dimension and then fed into the subsequent feature utilization network based on multi-layer perceptrons to obtain predictions of state value and exploration rate, respectively. Specifically, the differential calculation process described above can be represented as:

$$F_c^{(t)} = CNN(O_c^{(t)}), \hat{F}_c^{(t)} = CNN(\hat{O}_c^{(t)}) \quad (10)$$

$$\Delta F_c^{(t)} = Flatten(F_c^{(t)} - \hat{F}_c^{(t)}) \quad (11)$$

$$V(s^{(t)}) = MLP(\Delta F_c^{(t)}), \hat{y}^{(t)} = MLP(\Delta F_c^{(t)}) \quad (12)$$

Where $\Delta F_c^{(t)}$ is the vectorized difference of feature mappings, $V(s^{(t)})$ represents the state value, and $\hat{y}^{(t)}$ denotes the predicted exploration rate. It is worth noting that in the above equation, the CNN network shares parameters, while the MLP network does not. Through the processing of the network structure in the form of differences, the feature encoding network can be enhanced to some extent, thereby encoding key structural information in the environment into the feature mappings. The specific layers of the feature encoding network and the feature utilization network will be detailed in the experimental section of this paper.

2) *Asymmetric Actor-Critic Training Framework*: After completing the design of the structured feature extraction network, this paper proposes an asymmetric actor-critic training framework to train the network and ensure that the feature encoding network can accurately encode structural feature information. Regarding the specific design of the policy network, it will be detailed in the next section. This section mainly introduces the training framework. The asymmetric actor-critic training framework is mainly based on improvements to the PPO training framework, introducing a loss function from supervised learning, namely the exploration rate prediction loss function. Additionally, to enhance the stability of reinforcement learning training, this paper introduces a dynamically changing weight parameter for the exploration rate prediction loss function. This weight parameter decreases with the increase in training steps, so that the exploration rate prediction loss function only assists the training of the network in the early stages of training. As training progresses, its influence gradually diminishes, allowing the network training to be mainly completed by reinforcement learning.

Specifically, during training, multiple agents will interact with the environment according to the policy and collect data such as states, actions, and rewards into a data pool. After completing an interaction cycle, the algorithm will sample data of length from the data pool for training. During training, the loss function of the PPO algorithm can be represented as follows:

$$L^{PPO} = L^{CLIP}(\theta) - c_1 L^{VF}(\vartheta) + c_2 S[\pi_\theta] \quad (13)$$

Where $L^{CLIP}(\theta)$ represents the policy loss function, $L^{VF}(\vartheta)$ represents the value loss function, and $S[\pi_\theta]$ represents the entropy of the policy π_θ .

On this basis, this paper introduces the exploration rate prediction loss function as an additional loss function to supervise the training of the structured feature extraction network. During sampling, assuming the sampled data combination is denoted as $\{(s^{(t)}, y^{(t)})\}_{t=1:N_b}$, where $s^{(t)}$ refers to the privilege observation information and observation information at time t , and $y^{(t)}$ refers to the true exploration rate at time t . After $s^{(t)}$ is fed into the corresponding exploration rate prediction network, the predicted exploration rate $\hat{y}^{(t)}$ will be obtained. This prediction process can be understood as a regression fitting task, so during training, it is necessary to minimize the error between the true value and the predicted value. This paper adopts the mean squared error function as the loss function:

$$L^{Pre} = \frac{1}{N_b} \sum_{t=1}^{N_b} (y^{(t)} - \hat{y}^{(t)})^2 \quad (14)$$

The final loss function during training can be expressed as the weighted sum of the exploration rate prediction loss function and the PPO loss function:

$$L = L^{CLIP}(\theta) - c_1 L^{VF}(\vartheta) + c_2 S[\pi_\theta] - c_3 L^{Pre} \quad (15)$$

Where the weight c_3 is a function that gradually approaches 0 over time. In this paper, c_3 adopts a parameter-adjustable negative exponential function, denoted as $c_3 = \tilde{c}_3 e^{-k\tau}$, where \tilde{c}_3 and k are adjustable parameters (both greater than 0), and τ represents the size of the current accumulated training time steps.

The specific values of these parameters will be detailed in the experimental section of this paper. After obtaining the loss function L this paper trains the network based on this loss function through gradient ascent. By introducing the exploration rate prediction loss function, the feature encoding network obtains corresponding enhancements during the training process, thereby encoding the correct environmental structural feature information. This paper ultimately verifies the effectiveness of introducing this loss function through ablation experiments.

B. Design of Multi-Agent Decision Network Based on Topological Graph Matching

This section provides a detailed explanation of the multi-agent decision network based on topological graph matching adopted by multiple robots. After obtaining feature maps

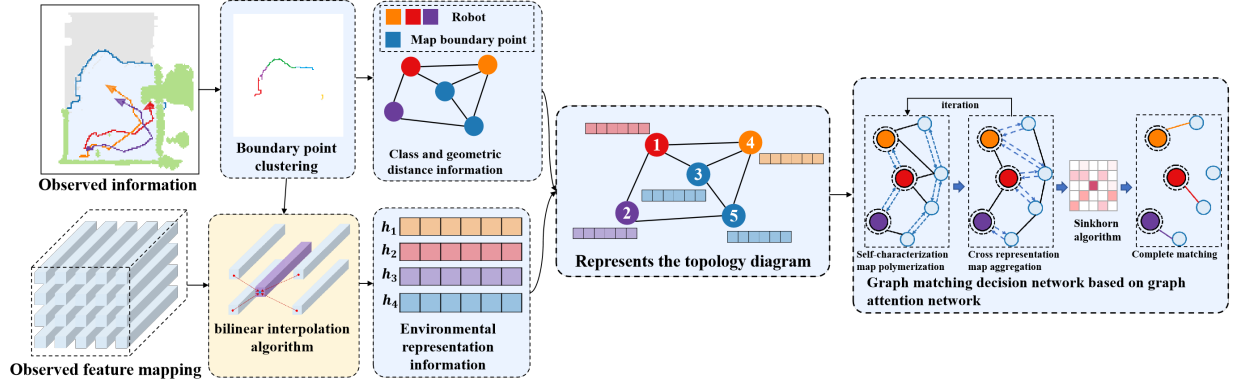


Fig. 6. Multi-agent decision-making network based on topological graph matching. This framework concatenates internal and external information fusion of the graph, completing graph matching between the representation of robots and boundary points, and assigning corresponding boundary points as long-term target points for each robot.

containing environmental structural feature information, this paper designs a single-point feature extraction method based on bilinear interpolation and boundary point clustering. This method extracts feature vectors corresponding to the positions of robots and boundary points in the observation feature map and combines them with distance geometric features extracted from the environment to construct a representation of the topological graph. Based on this representation of the topological graph, the subsequent decision network in this paper adopts a graph neural network framework, referencing the design in [19] as the network backbone. The overall framework process is illustrated in Fig. 6. It is worth noting that in the decision network, the feature maps utilized by multiple robots are observation feature maps, rather than privileged observation feature maps containing privileged information.

1) *Single Point Feature Extraction Method*: After obtaining feature maps containing environmental structural information, in order to utilize the information in the feature maps for decision-making, this paper proposes a single point feature extraction method based on nearest neighbor clustering and bilinear interpolation algorithm. This feature extraction method first clusters the boundary points and then utilizes the bilinear interpolation algorithm to extract features for each class of boundary points and the positions of robots in the feature map. The feature vectors obtained by single point feature extraction for boundary points and robot positions in the environment will serve as part of the corresponding node features in the final representation of the topological graph.

Specifically, to reduce computational complexity, this single point feature extraction method first clusters the boundary points, using the centroid of each cluster as the representative of that boundary point cluster, and also records the number of points in each cluster as one of the inputs for decision-making. Considering that in indoor mapping tasks, the environment structure mostly consists of combinations of rooms and corridors, boundary points are naturally divided into clusters by the walls of rooms and corridors. Typically, for a given cluster, exploration of the corresponding area can be achieved by a single robot. Therefore, this paper adopts a heuristic clustering method to cluster the boundary points in space: if two boundary points in space are adjacent in

Algorithm 1 Distance-based Adjacent Neighbor Clustering of Boundary Points

Input: A set of boundary points $F = \{f_k\}_{k=1:n}$ containing n boundary point.

Output: Boundary point cluster and corresponding cluster center point set $F_{cluster} = \{F_i, f_i^c\}_{i=1:n_c}$, where $F_i = \{f_i, f_i^c\}_i$.

Initializes the clustering of boundary points $F_{cluster}$;

while not $F = \emptyset$ **do**

Initialize a cluster, called F_i ;

Take a boundary point from the boundary point set F and add it to the cluster F_i

for p in set of boundary points **do**

if f is any neighboring boundary point of a cluster, and the distance to any boundary point within cluster F_i is less than r_{clus} . **then**

Remove f from the set F and add it to the cluster F_i .

end if

end for

Compute the average distance between each boundary point in the cluster F_i and the remaining boundary points in the cluster.

Select the boundary point with the smallest average distance as the cluster center point f_i^c .

Add the cluster F_i and the cluster center point f_i^c to the set of boundary point clusters $F_{cluster}$.

end while

the occupancy grid map, then these two boundary points are considered to belong to the same cluster. Additionally, the maximum distance between any two boundary points in the same cluster cannot exceed a threshold distance r_{clus} . In this paper, r_{clus} is set to the size of the robot's field of view radius. Therefore, after clustering is completed at time t , the boundary point cluster i can be represented as $F_i^{(t)} = \{f_k^{(t)}\}_{k=1:n_i}$ where $f_k^{(t)} \in \mathbb{R}^2$ represents the two-dimensional coordinates of boundary point K , and n_i indicates the number of boundary points in cluster i . Additionally, the centroid of boundary

point cluster $F_i^{(t)}$ can be represented as f_k^c . It is worth noting that, for simplicity, the term "boundary points" mentioned later in this chapter refers to the centroid points of the clustered boundary points. The specific clustering algorithm and computational process are illustrated in the pseudocode of Algorithm 1. As the observation feature map represents the structural features of the entire global scene, extracting the structural features of key locations such as robots and boundary points is necessary to introduce them into the decision-making network. To achieve this, this paper introduces a bilinear interpolation algorithm to interpolate the features in the feature map, thereby extracting the relevant feature vectors corresponding to the coordinates of the original grid map in the observation feature map. The schematic illustration of the interpolation algorithm is shown in Fig. 7. Specifically, given an input observation map size of $X \times Y \times 5$ and a feature map size of $X_l \times Y_l \times C_h$, for a point p_i with coordinates (x, y) in the input observation map, its projected coordinates in the feature map space should be $p'_i = (x', y')$, where $x' = x \cdot \frac{x_l}{x}$, $y' = y \cdot \frac{y_l}{y}$. The value corresponding to point (x', y') in the feature map $F_C^{(t)} \in \mathbb{R}^{X_l \times Y_l \times C_h}$ can be obtained using bilinear interpolation along the x-axis and y-axis directions. Let $x_0 = \lfloor x' \rfloor$, $x_1 = \lfloor x' \rfloor + 1$, and $y_0 = \lfloor y' \rfloor$, $y_1 = \lfloor y' \rfloor + 1$. Then, the boundary values $I_a \in \mathbb{R}^{C_h}$, $I_b \in \mathbb{R}^{C_h}$, $I_c \in \mathbb{R}^{C_h}$ and $I_d \in \mathbb{R}^{C_h}$ of the nearest feature vectors in the feature map to point (x', y') can be represented as follows:

$$I_a = F_C^{(t)}(x_0, y_0), I_b = F_C^{(t)}(x_0, y_1) \quad (16)$$

$$I_c = F_C^{(t)}(x_1, y_0), I_d = F_C^{(t)}(x_1, y_1) \quad (17)$$

In bilinear interpolation, the final feature value of the point is the weighted sum of its nearest boundary feature vectors, where the weights are determined by the distances between the projected point coordinates and the boundary point coordinates. Therefore, the weights w_a , w_b , w_c and w_d can be expressed as:

$$w_a = (x_1 - x') \cdot (y_1 - y'), w_b = (x_1 - x') \cdot (y' - y_0) \quad (18)$$

$$w_c = (x' - x_0) \cdot (y_1 - y'), w_d = (x' - x_0) \cdot (y' - y_0) \quad (19)$$

Finally, the feature vector I_i^f corresponding to the point $p_i = (x, y)$ in the observed feature map can be represented as:

$$I_i^f = w_a \cdot I_a + w_b \cdot I_b + w_c \cdot I_c + w_d \cdot I_d \quad (20)$$

The bilinear interpolation process described above is denoted as $I_i^f = \text{Interp}(p_i, F_C^{(t)})$ in this paper.

2) Construction of Topological Graph Representation:

Given the observation feature map, utilizes bilinear interpolation algorithm to extract feature vectors corresponding to the current positions of robots and boundary points in the original observation map. Then, these feature vectors are combined with geometric distance information in the environment to construct self-representation graphs $G_r = \{V_r, E_r\}$ and $G_f = \{V_f, E_f\}$ containing only robot or boundary point information, as well as the cross-representation graph $G_r = \{V_r, V_f, E_{rf}\}$ containing both robot and boundary point information.

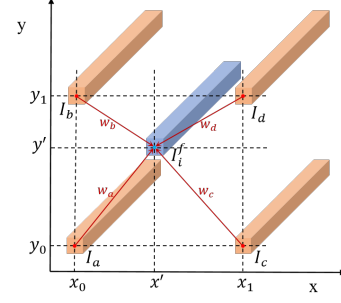


Fig. 7. Schematic diagram of bilinear interpolation algorithm.

For a node i in the self-representation or cross-representation graph, its initial node feature vector $v_i \in \mathbb{R}^{5+C_h}$ is composed of three parts: category information $v_i^{cla} \in \{0, 1\}^2$, geometric information $v_i^{geo} \in \mathbb{R}^3$, and environmental representation information $v_i^{env} \in \mathbb{R}^{C_h}$. The category information v_i^{cla} is a one-hot encoded label representing two categories: whether the node is a robot node or a boundary point. The first two dimensions of geometric information v_i^{geo} represent the node's position $p_i = (x, y)$, while the last dimension represents the geometric information of the node. If the node is a robot node, the geometric information is 0; if the node is a boundary point, the corresponding geometric information is the number of boundary points represented by the boundary point cluster. Additionally, the environmental representation information is obtained by interpolating the node's position information in the observation feature map: $v_i^{env} = \text{Interp}(p_i, F_C^{(t)})$. By processing each robot and boundary point in this way, node features containing environmental structure information and geometric distance information can be constructed for the self-representation and cross-representation graphs.

After constructing node features, the edges in the self-representation graph are fully connected. The initial values of these edges are not assigned, and their feature values are computed by the subsequent graph neural network based on the connected node features. In the cross-representation graph, a fully connected graph is formed between the robot nodes and boundary points, with an edge between each robot node and each boundary point. The initial feature values of edges in the cross-representation graph are the lengths of the shortest paths calculated by the fast marching algorithm between the corresponding robots and boundary points.

Furthermore, since the environment in this paper is partially observed, enhancing observations using historical observation information is beneficial for approximating the true state values of the local observations. Additionally, observing historical target points and the historical positions of robots can promote the dispersed movement of robots and reduce redundant exploration. Therefore, following the construction method of the aforementioned topological graphs, this paper also constructs the historical robot self-representation graph $G_r^h = \{V_r^h, E_r^h\}$ and the historical target point self-representation graph $G_g^h = \{V_g^h, E_g^h\}$ to represent the historical trajectory information of robots and historical boundary point information, respectively. To establish connections between

current robot and boundary point information and historical information, this paper also constructs the cross-representation graph $G_{r_r}^h = \{V_r^h, V_r, E_{r_r}^h\}$ between current robots and historical robot positions, as well as the cross-representation graph $G_{f_g}^h = \{V_g^h, V_f, E_{f_g}^h\}$ between current boundary points and historical target points. Through the construction of the aforementioned topological graphs, both structural feature information and geometric distance information in the environment can be adequately and robustly represented, laying the foundation for efficient decision-making by subsequent graph matching decision networks.

C. Graph Matching Decision Network Based on Graph Attention Network

After completing the construction of the topological graph representation, this paper adopted the network design from [19] as the network backbone to build a graph matching decision network based on the graph attention network. This decision network first utilizes a graph attention mechanism network to sequentially aggregate and extract features from the self-representation graph and the cross-representation graph, updating the features of corresponding edges and nodes in the topological graph. In the cross-representation graph G_{rf} after feature updating, the feature value of each edge in the edge set E_{rf} represents the matching degree of each robot node to the boundary point node. Therefore, this paper extracts the feature values from the updated edges E_{rf} and utilizes the Sinkhorn algorithm for linear assignment computation to achieve graph matching between the robot topological graph and the boundary point topological graph, assigning corresponding boundary points to each robot as long-term target points.

Specifically, for the self-representation graph, before the graph attention network performs feature extraction, this paper introduces an encoder based on a multi-layer perceptron network to encode the category information and geometric information $[V_i^{cla}, V_i^{geo}]$ of each node i in the graph, obtaining a feature vector of length C_h . This feature vector is concatenated with the environmental representation information V_i^{rep} to form the node feature $V_i^0 \in \mathbb{R}^{2C_h}$ for subsequent feature aggregation. The core idea of the graph attention network is to utilize an attention mechanism to aggregate features between neighboring nodes in the topological graph, and multi-hop information aggregation can be achieved through the concatenation of multiple layers of networks. Therefore, for the nodes $V_i^l \in \mathbb{R}^{h^l}$ in the l -th layer of the graph network, trainable weight parameters $W_k^l \in \mathbb{R}^{h_k^l \times h_l}$, $W_q^l \in \mathbb{R}^{h_q^l \times h_l}$, and $W_u^l \in \mathbb{R}^{h_u^l \times h_l}$ are introduced to generate the key $k_i^l \in \mathbb{R}^{h_k^l}$, query $q_i^l \in \mathbb{R}^{h_q^l}$, and value $u_i^l \in \mathbb{R}^{h_u^l}$ in the attention mechanism:

$$k_i^l = W_k^l \cdot V_i^l, q_i^l = W_q^l \cdot V_i^l, u_i^l = W_u^l \cdot V_i^l \quad (21)$$

In this paper, a dot-product style attention mechanism is employed for node aggregation in the self-representation graph. Therefore, the attention coefficient a_{ij}^l between node i and its neighboring node $j \in N_i$ can be calculated by the following equation:

$$a_{ij}^l = \frac{\exp(k_j^{lT} \cdot q_i^l)}{\sum_{m \in N_i} \exp(k_m^{lT} \cdot q_i^l)} \quad (22)$$

Additionally, the attention coefficient a_{ij}^l will also serve as the edge feature value between node i and its neighboring node j in the topological graph. Therefore, for node i , the aggregation of neighboring node feature values $V_{N_i}^l \in \mathbb{R}^{h_u^l}$ can be expressed as:

$$V_{N_i}^l = \sum_{m \in N_i} a_{im}^l \cdot u_m^l \quad (23)$$

The final feature value of node i will be updated as the aggregation of neighboring node features and the fusion with its own node feature:

$$V_i^{l+1} = v_i^l + \rho([V_i^l || V_{N_i}^l]) \quad (24)$$

In the above equation, $\rho(\cdot)$ represents the feature fusion function implemented using a multilayer perceptron, and $[||]$ denotes the concatenation of two feature values. Through this approach, the feature of each node in the self-representation graph will be updated to the aggregation of its own feature and the features of its neighboring nodes. This operation will be applied to the self-representation graphs G_r , G_f , G_r^h , and G_g^h in this paper.

After the completion of feature updates in all self-representation graphs, the node features will be used as the initial features of corresponding nodes in the cross-representation graph, which will then be fed into the subsequent graph attention network for feature extraction. The feature aggregation process in the cross-representation graph is the same as that in the self-representation graph. However, unlike the self-representation graph, the feature extraction in the cross-representation graph employs a non-linear mapping approach to generate attention coefficients. Additionally, the distance d_{ij} calculated by the fast marching algorithm is incorporated as an input to the non-linear mapping function $\varphi(\cdot)$:

$$a_{ij}^l = \frac{\exp(\varphi([k_j^l || q_i^l || d_{ij}]))}{\sum_{m \in N_i} \exp(\varphi([k_m^l || q_i^l || d_{im}]))} \quad (25)$$

The notation $[|| \cdot || \cdot]$ denotes the concatenation of three vectors. Additionally, the non-linear mapping function $\varphi(\cdot)$ is implemented using a multi-layer perceptron, which outputs a one-dimensional real number. In this study, the cross-representation graphs $G_{r_r}^h$, $G_{f_g}^h$, and G_{rf} will undergo sequential feature extraction using graph attention networks. It is worth noting that the complete feature extraction from self-representation graphs to cross-representation graphs, achieved by graph attention networks, will be considered as one layer of graph network extraction. Ultimately, multiple layers of graph network extraction modules will be concatenated to achieve comprehensive feature extraction.

After the feature extraction is completed, the edge features in the cross-representation graph G_{rf} will be extracted and used as the affinity matrix in graph matching, denoted as $A_M \in \mathbb{R}^{n_r \times n_f}$. Here, n_r and n_f represent the numbers of robots and boundary points, respectively. Each element in

the matrix represents the degree of matching between the corresponding robot and boundary point. Ultimately, this study employs the Sinkhorn algorithm to iteratively normalize the rows and columns of the affinity matrix alternately, gradually transforming it into a probability matrix to accomplish graph matching. Each robot will select the boundary point with the highest probability value from the probability matrix as its long-term target point.

D. Reinforcement Learning Related Designs

This chapter primarily focuses on the research of long-term target points in multi-robot active mapping tasks, employing a centralized decision-making approach. Therefore, this paper adopts the training paradigm of "centralized training, centralized execution," where multiple agents can be regarded as a centralized single agent with a multidimensional action space. In the reinforcement learning design, the observation space for the agents is a 5-channel map $O \in \{0, 1\}^{X \times Y \times 5}$. The action space for multiple agents is denoted as $A \in \{0, 1\}^{X \times Y \times n_r}$, where each agent's action involves selecting n_r grid points as long-term targets from a grid map of size $X \times Y$ and executing them in the next planning cycle. To address this problem, this paper employs an improved asymmetric actor-critic training framework based on the PPO algorithm. For reward design, this study adopts a simple and intuitive reward scheme: the more area multiple robots explore in a single planning cycle, the greater the reward obtained. Additionally, multiple robots will receive a fixed amount of penalty at each time step to encourage them to improve exploration efficiency. If the area explored by multiple robots at decision time is denoted as $A_e^{(t)}$, where $A_e^{(t)} = 0$, then the reward $r^{(t)}$ that robots can receive at time step $t (t > 0)$ can be represented as:

$$r^{(t)} = a_1(A_e^{(t)} - A_e^{(t-1)}) - a_2 \quad (26)$$

Where a_1 and a_2 are adjustable reward coefficients.

For the episode length in the reinforcement learning process, this paper sets a fixed maximum time step T as the episode length limit. It is noteworthy that in this chapter, the time required to execute one low-level action is referred to as a time step. If multiple agents complete full exploration of the environment within this time frame, meaning there are no reachable boundary points left in the environment, the episode ends. If multiple agents fail to complete exploration within the maximum time step, the episode ends when the maximum time step is reached. In this paper, the maximum time step for each episode during training is set to 1800, and the planning horizon for long-term target planning is set to 15 time steps.

V. EXPERIMENTAL RESULTS AND ANALYSIS

A. Experimental Setup

1) *Experimental Environment*: To validate the proposed framework, experiments were conducted using the iGibson physics simulation engine. iGibson is a virtual environment tool for robotics and AI research, providing realistic indoor scenes for the development and testing of robot perception, navigation, and task planning. The iGibson simulation engine

supports various map scene datasets and realistic physics-based interactions between robots and environments. In these experiments, TurtleBot robots equipped with depth cameras were used within the iGibson simulation engine to closely simulate real-world scenarios. The TurtleBot robots can move using a differential drive method and perceive the environment through depth cameras, with realistic collision interactions with the environment.

For the experiments, publicly available Gibson and MatterPort3D datasets were used for training and testing, respectively. The Gibson dataset offers large-scale 3D data of real indoor environments, while the MatterPort3D dataset provides a larger scale and more diverse set of indoor scenes. Nine scenes from the Gibson dataset were selected for training, and the trained model was then tested on the MatterPort3D dataset. Some scenes with small areas or disconnected regions that were impassable for the TurtleBot robots were excluded, resulting in 51 scenes for performance testing. These scenes were further divided into three subsets based on their area sizes: large, moderate, and small area scenes.

During testing, each scene underwent 100 tests, and the average results were recorded. The initial positions and orientations of the robots were randomly generated within the scene, with multiple robots initially concentrated in a small area.

2) *Parameter Settings and Training Details*: In this study, the grid map size was set to, where each grid cell represents an area of 0.01 square meters in the real world. The maximum field of view radius for the robot was set to 3 meters, and the maximum robot movement speed was set to 1 meter per second. During training, the maximum time steps per episode were set to 1800, and the planning horizon for long-term goal planning was set to 15 time steps. The coefficients α and β in the reward function were set to 0.005 and 0.225, respectively. The exploration rate prediction error ratio coefficients γ and δ were set to 0.05 and 0.01, respectively. The structure feature encoding network consisted of a 5-layer convolutional neural network concatenated, with the output observation feature mapping channel set to 32. The feature utilization network was a 3-layer multilayer perceptron network. Additionally, the multilayer perceptron network for encoding node categories and geometric information also had an output layer size of 32. Furthermore, in the graph matching decision network based on graph attention network, the vector lengths corresponding to the keys, values, and queries in the attention mechanism were set to 32. Both the feature fusion function and the non-linear mapping function were implemented using 4-layer multilayer perceptron networks. The code framework used in this study was the widely used PyTorch framework in academia. The asymmetric actor-critic training framework was an improvement based on the Proximal Policy Optimization (PPO) algorithm, with training hyperparameters set as shown in Table 1. The above training parameters were determined through experimental comparisons to obtain the optimal values. The code was deployed and trained on a workstation equipped with an Intel i9-12900k central processing unit and an NVIDIA GeForce RTX 4080 graphics card, with the complete training process taking approximately 72 hours.

TABLE I
TRAINING HYPERPARAMETER SETTINGS.

Hyperparameter name	value
Training rounds	1800
learning rate	1×10^{-5}
Incentive discount factor	0.99
GAE discount factor	0.95
Value loss function coefficient c_1	3.0
Strategy entropy coefficient c_2	1.0

3) *Evaluation Metrics*: The task considered in this chapter is active mapping in multi-robot indoor environments. For this task, this study evaluates the task completion effectiveness based on time efficiency and mapping completeness. Time efficiency is reflected in the time required for robots to complete exploration tasks, while mapping completeness is reflected in the exploration rate of the environment within a specified time. Therefore, this study adopts time steps and exploration rate as evaluation metrics. Time steps represent the time required for robots to complete exploration, while the exploration rate is the ratio of the area explored by the robot to the total explorable area of the environment within the specified maximum episode length.

B. Baseline Methods

To thoroughly validate the effectiveness of the proposed method, several high-performance baseline methods were introduced for comparison. These include four traditional planning methods (Utility [10], mTSP [5], Voronoi [3], CoScan [4]) and two reinforcement learning-based methods (Ans-Merge [1], NCM [19]). To ensure fair comparison, for the aforementioned baseline methods, only their top-level decision modules, which allocate long-term target points to robots, were utilized. The bottom-level action execution modules for all methods were uniformly processed using a fast traversal algorithm, and the planning horizons for long-term goals were kept the same for all methods. The following provides detailed introductions to the aforementioned baseline methods:

- 1) The Utility [10] method introduces the concept of information gain, where each robot selects the boundary point with the maximum information gain as the long-term target point. The information gain of a boundary point is defined as the area of unexplored regions within a circle centered at that boundary point with the robot's perception distance limit as the radius.
- 2) The mTSP [5] method transforms the multi-robot active mapping problem into a multiple Traveling Salesman Problem, which requires multiple robots to cooperatively traverse all boundary point nodes starting from their current node positions. This is achieved by establishing a boundary point-robot passable topological graph containing distance information. The Google-provided OR-Tools were used to solve this multiple Traveling Salesman Problem, and the first boundary point assigned to each robot was used as the long-term target point.

- 3) The Voronoi [3] method segments the entire map using the Voronoi partitioning method, with the robot's location as seed points. Each resulting map sub-block ensures that any point within it is closer to its corresponding seed point than to any other seed points. Each robot then selects the nearest boundary point within its map sub-block as the long-term target point.
- 4) The CoScan [4] method first performs K-means clustering on all boundary points and models the multi-robot active mapping task as an Optimal Mass Transport Problem, allocating boundary point clusters based on distances between robots and boundary point clusters. Finally, robots select the centroid of the assigned boundary point cluster as the long-term target point.
- 5) The Ans-Merge method extends the ANS [1] method, which is a reinforcement learning-based algorithm for single-robot exploration in unknown environments. It overlays the local grid map centered on itself and the global grid map as decision inputs and selects long-term target points for robots through regression. In this study, the original global grid map was expanded to a map merged by multiple robots, trained with the same reward setting as this study, and regression was used to generate long-term target points for each robot.
- 6) The NeuralCoMapping (NCM) [19] method builds a topological graph between boundary points and robots based solely on geometric distance information and introduces a multi-graph neural network to predict the neural distance between boundary points and robots. It then matches boundary points with robots based on neural distance and assigns long-term target points to each robot.

C. Performance Comparison Experiment

Based on the aforementioned experimental setup, this study implemented the related code and conducted training and testing in the iGibson simulation environment. During training, the number of robots in the scene was set to 3, the maximum episode length was set to 1800 time steps, and the planning interval for long-term target points was set to 15 time steps. This study recorded the number of time steps required for multiple robots to completely explore the environment during training as the training result. From the Fig.8, it can be observed that with the increase in training epochs, the number of time steps required for the ATR-Mapping algorithm and the NCM algorithm to complete the exploration task gradually decreases and eventually outperforms traditional planning methods. Among them, the ATR-Mapping algorithm slightly outperforms the NCM algorithm in terms of convergence speed and performance after convergence. Due to the small size of the scenes in the training set, with an average area of 48 square meters, the performance improvement effect of the ATR-Mapping algorithm cannot be fully reflected. It is worth noting that the Voronoi algorithm and the CoScan algorithm perform very similarly on the training set. The average step lengths for completing the exploration task are 486.55 and 488.89, respectively, so the corresponding two dashed lines in Fig.9 are very close.

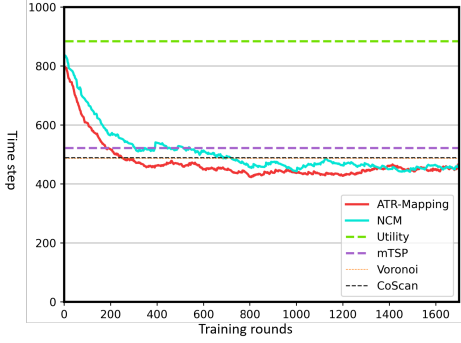


Fig. 8. Training performance comparison. The training results of the proposed ATR-Mapping and the baseline method NCM, as well as the comparison of the performance of the planning-based baseline methods (Utility, mTSP, Voronoi, and CoScan) on the training set.

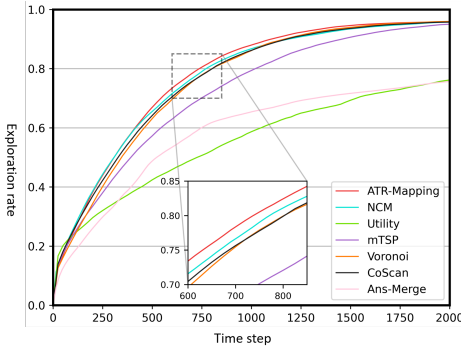


Fig. 9. Illustration of average exploration rate variation during test episodes.

To further validate the effectiveness of the proposed method, this study tested the trained models on the test set and compared them with baseline methods. During testing, the maximum episode length was set to 5000, and other settings remained the same as during training. The comparative experimental results are shown in Table 2. From the table, it can be observed that except for the Ans-Merge and Utility methods, all other methods achieve an exploration rate of over 95% in scenes of various area scales, indicating successful completion of full environment exploration. The Ans-Merge method, using the original grid map as input under the scenes and reward settings of this study, exhibited instability during training, resulting in poor model performance. The Utility method only considers information gain and ignores distance information, leading to significant path redundancy and difficulty achieving high exploration rates in large-scale scenes. However, in terms of time efficiency, the proposed ATR-Mapping outperforms various baseline methods in achieving relatively optimal efficiency under the same level of exploration rate. In moderate-sized and large-scale scenes, ATR-Mapping reduces the number of time steps required for mapping compared to the best-performing baseline method NCM by approximately 8%. The reason for this performance improvement lies in the fact that ATR-Mapping not only extracts distance information when representing the environment but also captures structural information and establishes a topological graph representation. Long-term goal planning based on such a representation,

which includes both distance geometric information and environmental structural information, is more reasonable, thus improving the efficiency of task completion.

D. Generalization Experiment

To verify the generalization ability of the proposed method in the face of different numbers of robots, the models trained with 3 robots were extended to settings with 4 and 5 robots for testing. The average test results on the entire test set are shown in Table 3. From the data in the table, it can be observed that despite the change in the number of robots during testing, the ATR-Mapping method proposed in this paper still achieves relatively superior time efficiency compared to the baseline methods. This generalization ability is believed to be to some extent attributed to the construction of the topological representation graph by ATR-Mapping. The topological representation graph not only contains environmental structural information obtained through interpolation but also includes the topological relationships and distance information between robots and boundary points. These topological relationships and distance information are less affected by changes in the number of robots, hence ATR-Mapping exhibits good generalization. Moreover, ATR-Mapping can also utilize environmental structural information from the topological representation graph to assist decision-making. Therefore, it can achieve higher decision efficiency based on good generalization. However, it can be observed that as the number of robots increases, the lead of the ATR-Mapping algorithm gradually decreases. This indicates that the ATR-Mapping model trained in only 9 scenes also has certain performance limitations in terms of generalization to the number of robots.

E. Ablation and Exploration Rate Prediction Experiments

To further validate the effectiveness of each module proposed in the ATR-Mapping method, this study conducted ablation experiments on different modules: exploration rate prediction loss function and observation feature mapping. The ablation experiments for the exploration rate prediction loss function and observation feature mapping are denoted as "w/o Prediction Loss Function" and "w/o Observation Feature Mapping," respectively. The comparison of training results after removing the respective modules is shown in Fig. 10, while the comparison test results of the trained models on the test set are presented in Table 4.

The experimental results indicate that after ablating the exploration rate prediction loss function, the algorithm's time efficiency decreases. This is reflected in both the training curves and the scene tests with three different sizes. Therefore, to some extent, this suggests that incorporating gradient back-propagation of the exploration rate prediction loss function during the training process of the critic module is beneficial for encoding correct and valuable feature information in the feature encoding module, thereby enhancing the decision-making efficiency of the robot.

Regarding the ablation experiment on the observation feature mapping, it refers to not using interpolation to introduce

TABLE II
PERFORMANCE COMPARISON IN MATTERPORT3D TEST DATASET.

methods	Small area scene ($< 60m^2$)		Medium area scene ($60 - 100m^2$)		Large-area scene ($> 100m^2$)	
	time step \uparrow	Exploration rate \downarrow	time step \uparrow	Exploration rate \downarrow	time step \uparrow	Exploration rate \downarrow
Utility[10]	1111.84	97.28	1779.78	95.41	3056.00	83.84
mTSP[5]	893.26	97.85	1120.22	96.76	1764.36	95.93
Voronoi[3]	904.53	97.68	1226.72	96.72	1520.07	96.19
CoScan[4]	716.63	98.09	1070.11	96.72	1601.43	96.07
Ans-Merge[1]	1529.58	96.08	2425.67	85.98	3827.21	81.19
NCM[19]	690.16	97.78	987.44	96.74	1492.07	96.09
ATR-Mapping	686.68	97.67	885.11	96.74	1369.29	96.03

TABLE III
COMPARATIVE EXPERIMENTAL PERFORMANCE ON GENERALIZATION OF ROBOT QUANTITIES.

methods	Number of robots=3		Number of robots=4		Number of robots=5	
	time step \uparrow	Exploration rate \downarrow	time step \uparrow	Exploration rate \downarrow	time step \uparrow	Exploration rate \downarrow
Utility[10]	1881.27	92.93	1681.73	93.69	1589.45	94.90
mTSP[5]	1212.49	96.94	1038.67	97.13	873.65	96.95
Voronoi[3]	1187.22	96.93	999.14	97.17	869.63	96.95
CoScan[4]	1084.27	97.05	988.78	97.18	835.63	97.00
Ans-Merge[1]	2476.57	88.43	1681.73	93.69	1536.73	95.00
NCM[19]	1015.22	96.95	868.67	97.01	761.78	97.00
ATR-Mapping	944.10	96.89	842.31	97.03	738.18	96.97

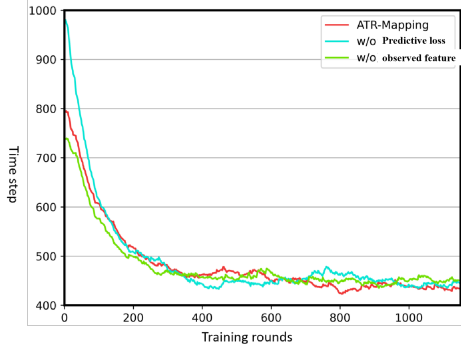


Fig. 10. Ablation experiment results of training for prediction loss function and feature map.

it into the decision-making module to form the representation topology map after obtaining the observation feature mapping in the critic module. Subsequently, the decision-making network uses a topology map containing only distance information for decision-making. From the training curves, it can be seen that removing the observation feature mapping accelerates the convergence speed of the training curves in the early stage. However, as training time increases, the final convergence position of the curves is not as good as that of the complete ATR-Mapping method. The experimental results on the test set also demonstrate that without using observation feature mapping, the decision-making efficiency of the robot decreases. Therefore, introducing the features from the observation feature mapping into the decision-making module by interpolation helps enhance the rationality of long-term target point selection for the robot, thereby improving the overall decision-making performance of the system.

Additionally, this paper also records the variation of the

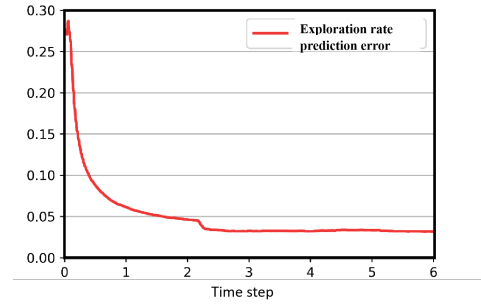


Fig. 11. Training curve of exploration rate prediction loss.

exploration rate prediction error with training time steps, as shown in Fig.11. The error loss function used in this paper is the mean squared error function. It can be observed that with the increase of training time steps, the error value rapidly decreases, corresponding to the rapid improvement in the accuracy of the exploration rate prediction network. The exploration rate reflects the difference between the privileged observation feature mapping and the observation feature mapping, which is the difference between the explored area and the overall explorable area. The exploration rate prediction network can accurately predict the exploration rate, which indirectly indicates that the feature encoding network can encode the environmental structural information reflected in the difference between the explored area and the overall explorable area.

VI. CONCLUSION

In this work, we propose a extraction of multi-robot environment features, this paper studies the active mapping problem of multi-robot and proposes a multi-robot active mapping method

TABLE IV
ABLATION EXPERIMENT RESULTS FOR PREDICTION LOSS FUNCTION AND FEATURE MAP.

methods	Small area scene ($< 60m^2$)		Medium area scene ($60 - 100m^2$)		Large-area scene ($> 100m^2$)	
	time step \uparrow	Exploration rate \downarrow	time step \uparrow	Exploration rate \downarrow	time step \uparrow	Exploration rate \downarrow
ATR-Mapping	686.68	97.67	885.11	96.74	1369.29	96.03
w/o Predictive loss function	692.47	97.72	950.00	96.67	1385.21	96.16
w/o Observed feature mapping	700.79	98.01	939.11	96.82	1421.36	96.20

based on asymmetric topological representation. This framework uses a differential structure feature extraction network and an asymmetric actor-critic training framework to obtain effective feature mapping for environmental feature information. For feature mapping, this paper designs a single-point feature extraction method based on bilinear interpolation and boundary point clustering to extract key point features, which are combined with geometric distance information to construct a topological representation graph. Based on the topological representation graph, this paper employs a decision network based on graph matching to assign corresponding boundary points as long-term target points for each robot to complete the decision-making process. Finally, this paper deploys and experiments with the proposed algorithms in simulation scenarios, and a large number of comparative experimental results demonstrate the effectiveness and advancement of the proposed methods.

REFERENCES

- [1] Devendra Singh Chaplot et al. "Learning to explore using active neural slam". In: *arXiv preprint arXiv:2004.05155* (2020).
- [2] Kevin Chen et al. "Topological planning with transformers for vision-and-language navigation". In: *Proceedings of the IEEE/CVF Conference on Computer Vision and Pattern Recognition*. 2021, pp. 11276–11286.
- [3] Rafael Gonçalves Colares and Luiz Chaimowicz. "The next frontier: Combining information gain and distance cost for decentralized multi-robot exploration". In: *Proceedings of the 31st Annual ACM Symposium on Applied Computing*. 2016, pp. 268–274.
- [4] Siyan Dong et al. "Multi-robot collaborative dense scene reconstruction". In: *ACM Transactions on Graphics (TOG)* 38.4 (2019), pp. 1–16.
- [5] Jan Faigl, Miroslav Kulich, and Libor Přebí. "Goal assignment using distance cost in multi-robot exploration". In: *2012 IEEE/RSJ International Conference on Intelligent Robots and Systems*. IEEE. 2012, pp. 3741–3746.
- [6] Juliane Fischer et al. "Design, application, and evaluation of a multi-agent system in the logistics domain". In: *IEEE Transactions on Automation Science and Engineering* 17.3 (2020), pp. 1283–1296.
- [7] Mingyang Geng et al. "Learning to cooperate in decentralized multi-robot exploration of dynamic environments". In: *Neural Information Processing: 25th International Conference, ICONIP 2018, Siem Reap, Cambodia, December 13–16, 2018, Proceedings, Part VII* 25. Springer. 2018, pp. 40–51.
- [8] Mingyang Geng et al. "Learning to cooperate via an attention-based communication neural network in decentralized multi-robot exploration". In: *Entropy* 21.3 (2019), p. 294.
- [9] Geoffrey A Hollinger et al. "Distributed data fusion for multirobot search". In: *IEEE Transactions on Robotics* 31.1 (2014), pp. 55–66.
- [10] Miguel Juliá, Arturo Gil, and Oscar Reinoso. "A comparison of path planning strategies for autonomous exploration and mapping of unknown environments". In: *Autonomous Robots* 33 (2012), pp. 427–444.
- [11] Haye Lau. "Behavioural approach for multi-robot exploration". In: *Australasian Conference on Robotics and Automation*. Australian Robotics and Automation Association Inc. 2003.
- [12] Tsung-Ming Liu and Damian M Lyons. "Leveraging area bounds information for autonomous decentralized multi-robot exploration". In: *Robotics and Autonomous Systems* 74 (2015), pp. 66–78.
- [13] Ragesh Kumar Ramachandran et al. "Resilient monitoring in heterogeneous multi-robot systems through network reconfiguration". In: *IEEE Transactions on Robotics* 38.1 (2021), pp. 126–138.
- [14] Alessandro Renzaglia and Agostino Martinelli. "Potential field based approach for coordinate exploration with a multi-robot team". In: *2010 IEEE Safety Security and Rescue Robotics*. IEEE. 2010, pp. 1–6.
- [15] James A Sethian. "Fast marching methods". In: *SIAM review* 41.2 (1999), pp. 199–235.
- [16] Aaron Hao Tan et al. "Deep reinforcement learning for decentralized multi-robot exploration with macro actions". In: *IEEE Transactions on Automation Letters* 8.1 (2022), pp. 272–279.
- [17] Alberto Vergnano et al. "Modeling and optimization of energy consumption in cooperative multi-robot systems". In: *IEEE Transactions on Automation Science and Engineering* 9.2 (2012), pp. 423–428.
- [18] Brian Yamauchi. "A frontier-based approach for autonomous exploration". In: *Proceedings 1997 IEEE International Symposium on Computational Intelligence in Robotics and Automation CIRA'97. Towards New Computational Principles for Robotics and Automation*. IEEE. 1997, pp. 146–151.
- [19] Kai Ye et al. "Multi-robot active mapping via neural bipartite graph matching". In: *Proceedings of the IEEE/CVF Conference on Computer Vision and Pattern Recognition*. 2022, pp. 14839–14848.
- [20] Jincheng Yu et al. "Smmr-explore: Submap-based multi-robot exploration system with multi-robot multi-target potential field exploration method". In: *2021 IEEE International Conference on Robotics and Automation (ICRA)*. IEEE. 2021, pp. 8779–8785.
- [21] Lin Zhang et al. "Digital-twin prediction of metamorphic object transportation by multi-robots with thz communication framework". In: *IEEE Transactions on Intelligent Transportation Systems* (2022).